Letter

Spin-flip-driven giant magnetotransport in A-type antiferromagnet $NaCrTe_2$

Junjie Wang,[1,2] Jun Deng,[1,2] Xiaowei Liang,[3] Guoying Gao,[3,*] Tianping Ying,[4] Shangjie Tian,[5] Hechang Lei,[5] Yanpeng Song,[1] Xu Chen,[1] Jian-gang Guo,[1,6,†] and Xiaolong Chen[1,2,6,‡]

[1]*Beijing National Laboratory for Condensed Matter Physics, Institute of Physics, Chinese Academy of Sciences, Beijing 100190, China*

[2]*University of Chinese Academy of Sciences, Beijing 100049, China*

[3]*Center for High Pressure Science, State Key Laboratory of Metastable Materials Science and Technology, Yanshan University, Qinhuangdao 066004, China*

[4]*Materials Research Center for Element Strategy, Tokyo Institute of Technology, Yokohama 226-8503, Japan*

[5]*Department of Physics and Beijing Key Laboratory of Opto-electronic Functional Materials & Micro-nano Devices, Renmin University of China, Beijing 100872, China*

[6]*Songshan Lake Materials Laboratory, Dongguan, Guangdong 523808, China*

(Received 10 December 2020; revised 13 July 2021; accepted 8 September 2021; published 29 September 2021)

The value of angle-dependent magnetoresistance (MR) synergistically and simultaneously depends on the magnitudes of magnetoresistance (MR) and magnetocrystalline anisotropy energy (MAE). In a magnetic material, the concurrence of gigantic angle-dependent MR and MR signals is rather difficult due to weak spin-lattice coupling and small MAE. Here we report the considerable magnetotransport effect in layered A-type antiferromagnetic (AFM) $NaCrTe_2$ by realigning the spin configurations. Above 3 (8) T, the antiparallel spins of adjacent layers experience a spin-flip transition to a parallel alignment along the c axis (ab plane). Theoretical calculations reveal that the energy band gap narrows from 0.39 to 0.11 eV, accompanying a transition from semiconductor (high-R state) and half semiconductor (low-R state), respectively. Thus, a gigantic negative MR ratio of -90% is obtained at 10 K. More importantly, the decrement of R along $H \parallel c$ is far quicker than that of $H \parallel ab$ because the MAE of the Ising-like ferromagnetic (FM) state is 1017 μeV/Cr^{3+} lower than that of XY-like FM. The distinct trends result in the angle-dependent MR ratio of 732% at 10 K. These findings unravel the intrinsic origin of magnetoresistance in $NaCrTe_2$ and will stimulate us to explore the H-sensitive transport property in more AFM materials.

DOI: 10.1103/PhysRevMaterials.5.L091401

I. INTRODUCTION

Angle-dependent magnetoresistance (MR) originates from the relativistic spin-orbit coupling (SOC) in magnetic materials, which is inherently determined by the variation of conductivity and density of states at the Fermi level (E_F) under H [1]. Normally, the resistance (R) is dependent on the relative angle between the electric current (J) or crystallographic axes and H, where the R under parallel H is usually larger than that of the perpendicular direction in a ferromagnetic alloy. The angle-dependent MR magnitudes of a few percent (<5%) are found in known ferromagnetic permalloy [2]. For practical applications, this kind of spin-dependent transport property has enormous technological importance, particularly in fabricating magnetic memory devices for recording [3] and sensors [4].

Exploring strong angle-dependent MR in antiferromagnetic (AFM) materials has been attracting intensive interest due to their superior properties such flipped spin, reduced stray field, and fast spin dynamics [5,6]. However, altering the AFM ordering and controlling the R in antiferromagnets by H is generally difficult, usually leading to a weak angle-dependent MR signal. This has been reported in a series of collinear AFM alloys and compounds such as FeRh [7], CuMnAs [8], and MnTe [9]. Few AFM materials with large angle-dependent MR values have been identified. In AFM oxides $La_{2-x}Sr_xCuO_4$ [10] and $Pr_{1.3-x}La_{0.7}Ce_xCuO_4$ [11], strong coupling between spin and lattice modifies the electronic structure as in-plane spin-flop transitions happen. This kind of H-direction-dependent conductivity leads to an angle-dependent MR ratio of 28%. Recently, another $J = 1/2$ AFM layered semiconductor Sr_2IrO_4 is intensively investigated, in which the angle-dependent MR signal is observed in the regime of in-plane metamagnetic transition [12–15]. In the latest report, the largest angle-dependent MR ratio of 160% is achieved in high-quality Sr_2IrO_4 single crystal [16]. Theoretical calculations reveal that as the net spins of Ir^{4+} change from the [110] to the [100] axis, the energy band gap (E_g) of 35.0 meV decreases to 25.9 meV. The H-dependent electronic structure is also the main origin of angle-dependent MR. Based on the above analyses, it is suggested that the easy-flipped magnetic order in AFM compounds is a decisive factor in turn tuning conductivity and inducing large angle-dependent MR.

As for different magnetic orders in antiferromagnets, the A-type AFM state is the simplest one with intralayer ferromagnetic (FM) and interlayer AFM coupling, as shown in Fig. 1(a). There are two spin-flip fields, H_{sf1} and H_{sf2}, along

*gaoguoying@ysu.edu.cn
†jgguo@iphy.ac.cn
‡xlchen@iphy.ac.cn

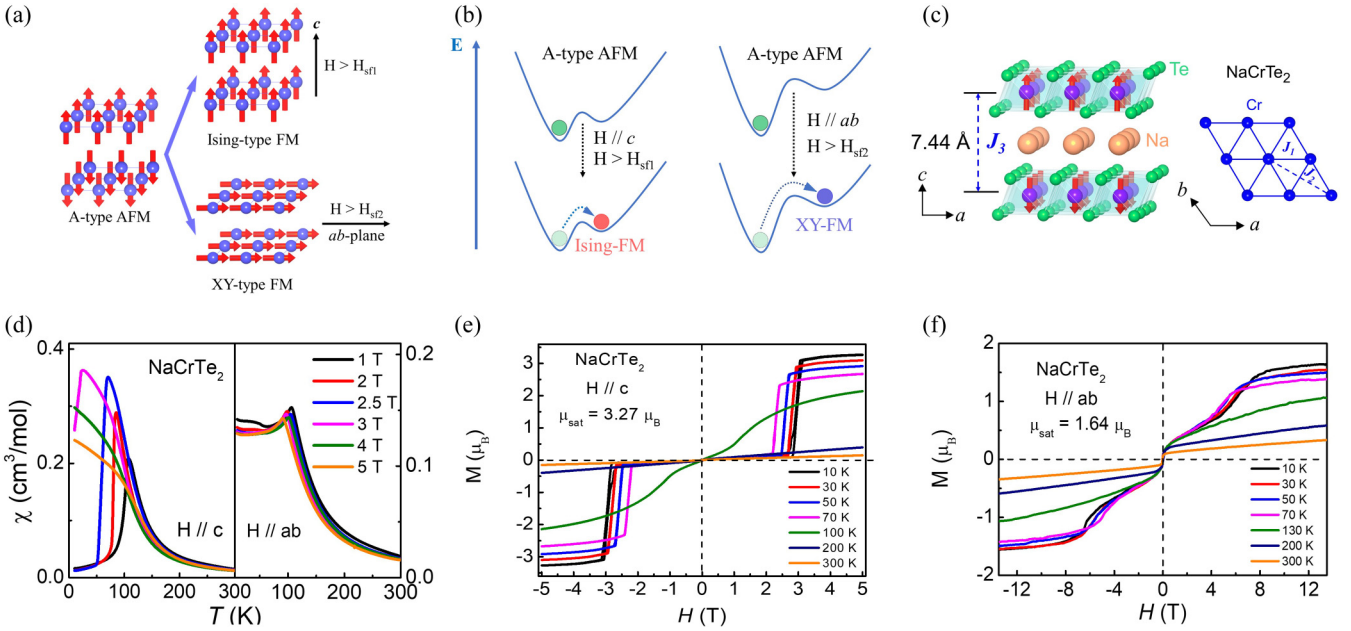

FIG. 1. Spin-flipped transition of A-type antiferromagnet $NaCrTe_2$. (a) Spin-flip transition in an A-type layered antiferromagnet under H. By applying large enough H along the easy axis and the hard axis, two kinds of FM states can be obtained. (b) Relative total energy of A-type AFM, Ising-like type FM and XY-like type FM. (c) Crystal structure of $NaCrTe_2$. Blue ball is Cr, green ball Te, and orange ball Na. Interlayer spacing is 7.44 Å. Right panel shows a single Cr layer. J_1, J_2, and J_3 represent the nearest neighbor, the next-nearest neighbor, and interlayer magnetic exchange constants, respectively. (d) Temperature dependence of magnetic susceptibility (χ) of $NaCrTe_2$ under $H \parallel c$ and $H \parallel ab$. [(e),(f)] Isothermal M-H curves of $NaCrTe_2$ under $H \parallel c$ and $H \parallel ab$.

the magnetic easy axis (out of plane) and hard axis (in plane), respectively. Under $H > H_{sf1}$, the A-type AFM coupling will change into an Ising-like FM state, where all the spins of the atoms point to the c axis, while for $H > H_{sf2}$, the spin directions lie in the ab plane, leading to a XY-like FM state. In terms of energy E, the A-type AFM has the lowest energy. Both FM alignments are excited states, in which the energy of the Ising-type FM state is lower than that of the XY-type FM, as depicted in Fig. 1(b). This is like the effect of giant magnetoresistance (GMR), where the change of magnetic coupling leads to different resistances.

Following this anticipated outcome, we synthesize the single crystal of $NaCrTe_2$ with layered A-type AFM order and investigate its low-temperature magnetotransport properties. As H exceeds the spin-flip fields H_{sf} of the easy axis (3.2 T) and the hard axis (13.0 T), the antiparallel spins of adjacent layers realign to Ising-like FM and XY-like FM, respectively. Meanwhile, the calculated E_g decreases from 0.39 eV (high-R state) to 0.11 eV (low-R state). The enhanced conductivity results in a negative MR of -90%. Furthermore, owing to the large MAE between the two FM states, the descending trends from high R to low R are far different, resulting in the very high angle-dependent MR ratio of 732%. Our works highlight the importance of narrow band gap antiferromagnets for exploring H-sensitive magnetoproperties.

II. EXPERIMENT

Stoichiometric amounts of Na, Cr, and Te were mixed and loaded into an alumina crucible that was sealed into an evacuated quartz tube backfilled with 0.2 atm of argon. The assembly was heated to 1000 K with a duration of 25 h. After that, the sintered sample was taken out, reground, pelletized, and reheated to 1000 K for 25 h for homogeneity. For growing a $NaCrTe_2$ single crystal, the sealed quartz tube was heated to 1200 K with a duration of 20 h, slowly cooled to 1000 K with a rate of 3 K/h. Then it was finally furnace cooled to room temperature. A single crystal with a shiny surface and a size of $1.5 \times 1.5 \times 0.1\ mm^3$ was obtained. All the procedures were handled in a glove box filled with argon gas.

Powder x-ray diffraction (PXRD) patterns were collected using a PANalytical X'Pert PRO diffractometer (Cu $K\alpha$ radiation) with a graphite monochromator in the reflection mode. Rietveld refinement of the PXRD pattern was performed using FULLPROF software suites [17]. The scanning electron microscopy (SEM) image of the sample was captured from a Hitachi S-4800 field emission scanning electron microscope (FE SEM). The composition was determined by energy dispersive spectroscopy (EDS) with an average of ten sets of data. Electrical resistivity (ρ) and Hall resistivity (ρ_{xy}) were measured through the standard six-wire method using a physical property measurement system (PPMS-9T and -14T, Quantum Design), respectively. Magnetic properties were measured through the vibrating sample magnetometer (VSM) option in the PPMS-9T and PPMS-14T (Quantum Design).

First principles calculations were performed with the Vienna *ab initio* simulation package (VASP) [18]. We adopted the generalized gradient approximation (GGA) in the form of Perdew-Burke-Ernzerhof (PBE) [19] and HSE06 [20] for the exchange-correlation potentials. A Hubbard $U = 3$ eV was adopted for the Cr $3d$ orbital. The projector augmented wave (PAW) pseudopotentials were used with a plane-wave energy of 500 eV. The $2p^6 3s^1$, $3d^5 4s^1$, and

TABLE I. Optimized lattice constants of $NaCrTe_2$ with A-type AFM and Ising-like type FM state; total energy of $2 \times \sqrt{3}$ supercell (GGA+U+SOC); band gap E_g; magnetic coupling constants J_1, J_2, and J_3; magnetic anisotropy energy (MAE); Néel temperature (T_N); and Curie temperature (T_c').

$NaCrTe_2$	a (Å)	c (Å)	E_{total} (eV)	E_g (meV)	J_1 (meV)	J_2 (meV)	J_3 (meV)	MAE (μeV per Cr^{3+})	T_N (K)	T_c' (K)
A-type AFM	4.0053	7.4458	−140.8182	0.39	2.98	1.86	−0.08	–	110	–
Ising-like FM	4.1412	7.3941	−140.8123	0.11	–	–	–	1017	–	113

$5s^2 5p^4$ electron configurations were treated as valence electrons for Na, Cr, and Te, respectively. A Monkhorst-Pack Brillouin zone sampling grid with a resolution of $0.02 \times 2\pi$ Å^{-1} was applied. Parameters were relaxed until all the forces on the ions were less than 10^{-3} eV/Å. Phonon spectra were calculated using the finite displacement method implemented in the PHONOPY code [21] to determine the dynamical stability of the studied structures. The magnetism is described by the classical Heisenberg Hamiltonian $H = -J_1 \sum_{i,j} S_i S_j - J_2 \sum_{i,j} S_i S_j - J_3 \sum_{i,j} S_i S_j$, where J_1 is the nearest neighbor, J_2 the next-nearest neighbor, and J_3 the interlayer coupling constant, respectively. These constants can be extracted from the total energy of different magnetic structures.

III. RESULTS AND DISCUSSION

A. Spin-flip transitions in $NaCrTe_2$

Figure 1(c) shows the crystal structure of A-type AFM $NaCrTe_2$, in which the $CrTe_6$ octahedrons are edge shared in a $CrTe_2$ layer and the Na ions locate between $CrTe_2$ layers. The Rietveld refinements of the PXRD pattern of $NaCrTe_2$ are shown in Fig. S1(a) in the Supplemental Material [22]. $NaCrTe_2$ crystallizes in the space group of P-3m1 with $a = 4.0053$ Å and $c = 7.4485$ Å. Based on the formation enthalpies and phonon spectra shown in Figs. S1(b)–S1(d) [22], the composition and structure of $NaCrTe_2$ are thermodynamically stable. We calculate the total energy of both FM states and three other AFM states by using a $2 \times \sqrt{3}$ supercell (Fig. S2 [22]). For the A-type AFM, the extracted magnetic exchange constants of the J_1, J_2, and J_3 are 2.98, 1.86, and −0.08 meV; see Table I. These values indicate that the intralayer and interlayer magnetic coupling are FM and AFM, respectively, and the interlayer interaction is very weak. Furthermore, it is found that the A-type AFM has the lowest energy of −140.8182 eV. The Ising-like-FM and XY-like-FM states are 5.9 and 19.8 meV higher in energy, respectively.

A high-quality $NaCrTe_2$ single crystal is grown by the self-flux method, and its PXRD pattern and optical image are shown in Fig. S3(a) [22]. The EDS spectra and chemical-element mapping confirm that the atomic ratio is close to 1:1:2 as shown in Figs. S3(b)–S3(f) [22]. The temperature-dependent magnetic susceptibility (χ) of $NaCrTe_2$ single crystal under $H \parallel c$ and $H \parallel ab$ is plotted in Fig. 1(d). At $H = 1$ T, the features of the χ-T curves indicate that intralayer and interlayer interactions are FM and AFM couplings, respectively, and the Néel temperature T_N is 106 K. It matches the above prediction and another report [23]. In Fig. S4, the effective moment μ_{eff} per Cr^{3+} obtained from Curie-Weiss fitting is 3.91 μ_B for $H \parallel c$, which is consistent with the spin-only moment (3.88 μ_B) in a free Cr^{3+} ion. The fitting equations are shown in the Supplemental Material (SM), section S1 [22]. As H increases along the c axis, the T_N gradually lowers. As $H > 3$ T, the AFM transition totally disappears, and then an H-induced FM transition emerges. The χ in the ab plane, however, is hardly suppressed as H increases to 5 T. The M-H curves in Figs. 1(e) and 1(f) exhibit paramagnetic (PM) behaviors at $T > T_N$, while the M abruptly jumps to saturated values in the range of $2\,\text{T} < H < 3\,\text{T}$ below T_N with $H \parallel c$, indicating a transition from A-type AFM to Ising-type FM along the c axis. At $H = 5$ T, the saturated FM moment is 3.27 μ_B at 10 K. For $H \parallel ab$, it also exhibits spin-flip transition from A-type AFM to XY-type FM below T_N, and the moment slowly increases and then saturates to 1.64 μ_B at 10 K as $H > 8$ T.

B. MR and angle-dependent MR

Figures 2(a) and 2(b) show the temperature-dependent in-plane ρ_{ab} and out of plane ρ_c under $H \parallel c$. At low H, there are large jumps in the ρ_{ab} and ρ_c curves at T_N, which are associated with metal-insulator transition (MIT)-like transition due to the formation of A-type AFM ordering. As H increases, the T_N gradually shifts to low temperatures and the amplitude of resistivity jump decreases. At $H > 3$ T, this resistivity jump is suppressed, and then the small kinks in ρ_{ab} and ρ_c show up. It might be viewed as manifestations of the H-induced FM transition. The derivation of ρ_{ab} and ρ_c of $H = 5$ T are shown in Fig. S5 [22], in which the peaks due to the FM-like state locate at $T_c' = 113$-122 K. In Figs. 2(c) and 2(d), we show the isothermal in-plane MR of $NaCrTe_2$ over a broad T (10–300 K) and H (up to 14 T) along magnetic c axis and ab plane. Here we define the MR ratio as

$$\text{MR} = \frac{\rho(\text{H}) - \rho(0)}{\rho(0)} \times 100\%.$$

We find that, at $T > T_N$, the absolute value of MR is generally small. Below $T < T_N$, a kind of steplike decrement in MR happens as $H > H_{sf1}$, resulting in negative MR effects along both directions. The maximal MR_{ab} are −81.6% and −78.5% at 10 K under $H \parallel c$ and $H \parallel ab$. The maximal MR_c are as large as −87.9% and −90.6% for $H \parallel c$ and $H \parallel ab$ as shown in Figs. S6(a) and S6(b) [22], respectively. Such MR is intimately linked to the different conductivity between the AFM and FM states of $NaCrTe_2$. Therefore, we measured the H-dependent Hall resistivity ρ_{xy} from 10 to 300 K and calculated carrier concentration n based on a single-band

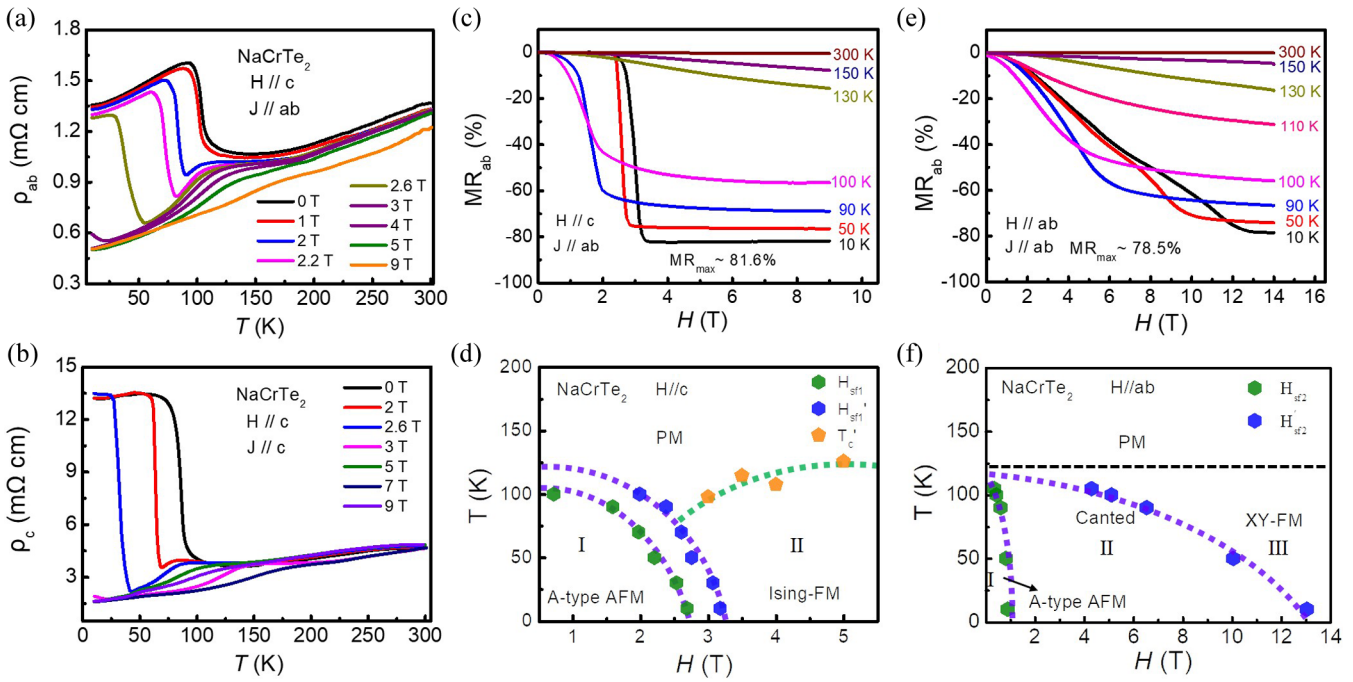

FIG. 2. Electrical transport and magnetoresistance (MR) of $NaCrTe_2$ single crystal. [(a),(b)] T-dependent electrical resistivity ρ_{ab} and ρ_c under $H \parallel c$. With increasing H, the jump due to PM to AFM transition is gradually suppressed. [(c),(d)] Isothermal MR_{ab} ($J \parallel ab$) of $NaCrTe_2$ under $H \parallel c$ and $H \parallel ab$. [(e),(f)] Magnetic phase diagrams in $NaCrTe_2$ under $H \parallel c$ and $H \parallel ab$. The data are taken from the onset H (H_{sf1}, green) of R drop and onset H (H'_{sf1}, blue) of low-R state. H-induced FM transition temperature T'_c (orange) is determined from the derivative of the M-T curves at high H.

model. The data are plotted in Figs. S6(c) and S6(d) [22]. The fitting equations are shown in SM, section S2 [22]. Under the PM state, the H-dependent ρ_{xy} is linear. Under low H, the slope abruptly increases below T_N, suggesting that the n of the AFM state reduces. Under high H, the slope of low-T curves inversely lowers, indicating that the n increases after transitioning into the FM phase. The magnitudes of n increase from $7 \times 10^{19}\,\mathrm{cm}^{-3}$ to $1.3 \times 10^{20}\,\mathrm{cm}^{-3}$, which correspond to the high R of the AFM state and the low R of the FM state, respectively.

On the other hand, we find that the decrement of R along $H \parallel c$ is remarkably quicker than that of $H \parallel ab$. It implies that the A-type AFM is easier flipped to Ising-like-type FM than XY-like-type FM, evidenced by the smaller H_{sf1}. In Figs. 2(e) and 2(f), two magnetic phase diagrams are plotted based on the data taken from the MR and χ-T curves. We can see that the A-type AFM firstly transitions to an intermediate phase and then changes into Ising-like type FM or XY-like type FM as H increases. Along $H \parallel c$, there is a small gap of 0.5 T between H_{sf1} and H'_{sf1}, while the gap between H_{sf2} and H'_{sf2} is 12 T for $H \parallel ab$. It clearly explains the anisotropy in the process of flipping the A-type AFM state. In the intermediate phase, there may exist a mixed spin structure or canted FM phase like the observation in $CrPS_4$ [24].

To check the angle-dependent MR in $NaCrTe_2$, we systematically measured the angle-dependent MR curves and plotted the data of selected temperatures in Fig. 3. Supplemental angle-dependent MR data can be seen in Figs. S7 and S8 [22]. Here the angle-dependent MR ratio is defined as

$$\mathrm{MR} = \frac{\rho(\mathrm{H}) - \rho(0)}{\rho(0)} \times 100\%$$

at each temperature, where $R_{\max}$ and $R_{\min}$ are the maximal and minimal values for a given field as θ sweeping from 0° to 360°. The measured schemes are drawn in the inset of Figs. 3(c) and 3(d). At $T > T_N$, such as 130 K, the $NaCrTe_2$ is under the PM state, and the R_{ab} shows a weakly angle-dependent variation as shown in Fig. S7(a) [22]. The resultant angle-dependent MR of 5 T is 6.3%, which is comparable to those values in many FM materials [25] and conventional AFM semiconductors [26]. At $T = 90\,\mathrm{K}$, just below T_N, the R_{ab} of $H = 1\,\mathrm{T}$ initially increases and then decreases, exhibiting twofold symmetry with maximal values at $\theta = 90°$ and 270° and minimal values at $\theta = 0°$ and 180°. At $H = 2.7\,\mathrm{T}$ and $\theta = 0°$, the magnetic coupling is A-type AFM and thus the R_{ab} is at the high-R state. Increasing θ to the flipped angle $\theta_f = 30°$, the coupling changes into the Ising-like FM state, so the R_{ab} slowly lowers and then keeps the low-R state from 45° to 135°. At larger θ, the R_{ab} recovers and repeats the oscillations with twofold symmetry plus R plateau. Meanwhile, the R oscillation exhibits the largest amplitude at $H = 2.7\,\mathrm{T}$. Under $H = 9\,\mathrm{T}$, the twofold symmetry still survives while the oscillated magnitude becomes weaker again. These features are more remarkable at $T = 10\,\mathrm{K}$; see right panel of Fig. 3(a). All the curves exhibit twofold symmetry while having wider plateaus because the θ_f moves to 60°. It means that at lower temperatures, one needs a stronger H component along the c axis to align all the spins to the Ising-type FM form. In Fig. 3(b), the periodic oscillation of R_c are almost similar to those of R_{ab} except for the amplitude. We summarize the H-dependent angle-dependent MR ratios of R_{ab} and R_c in Figs. 3(c) and 3(d). For R_{ab} and R_c, the angle-dependent MR signal are pretty small below H_{sf1}, and then quickly reach

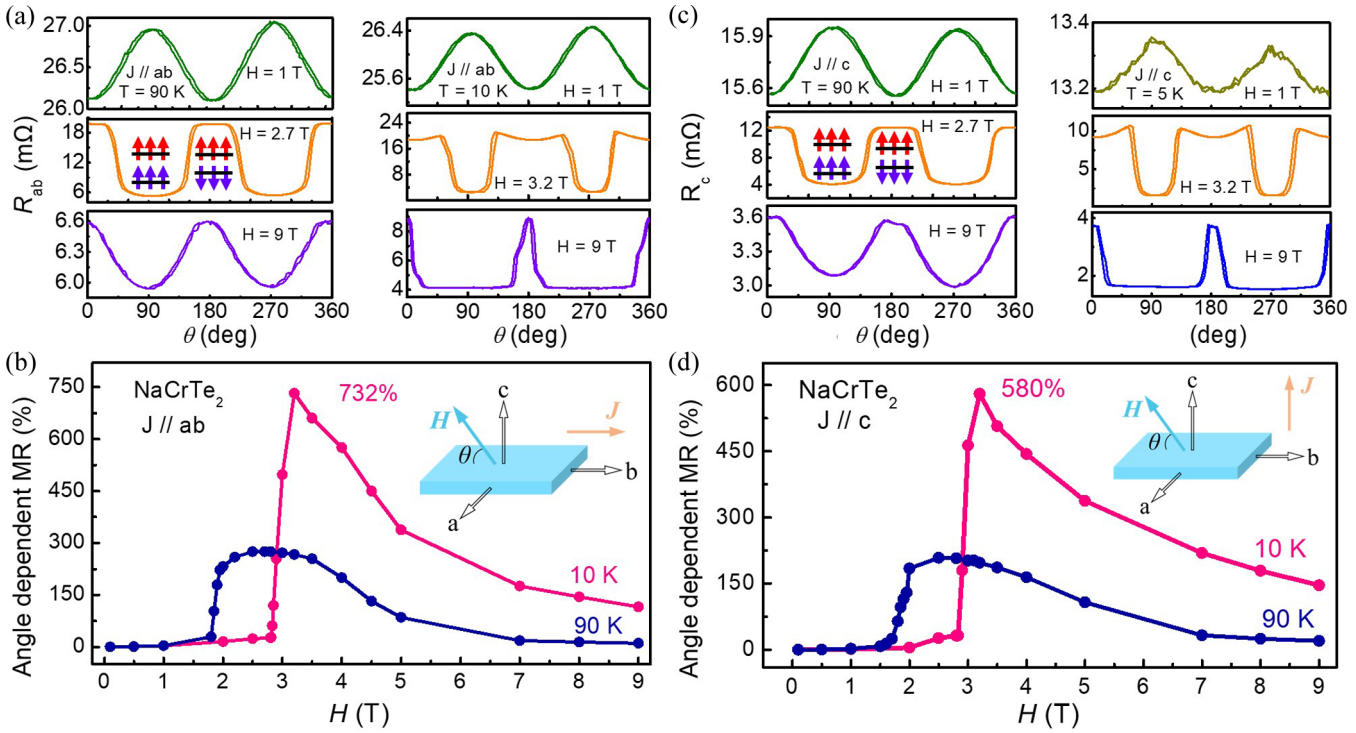

FIG. 3. Anisotropic magnetoresistances of $NaCrTe_2$ single crystal. (a) R_{ab} of $NaCrTe_2$ single crystal (sample 1) under various H at 90 and 10 K. (b) R_c of $NaCrTe_2$ single crystal (sample #) under various H at 90 and 10 K. The data at selected H are presented for clarity. Inset arrows show schematic spin alignments under given H and angle. [(c),(d)] Giant angle-dependent MR ratios are observed in R_{ab} and R_c. Insets are the schematic geometry of the relative orientation between current (J), magnetic field (H), and crystal axis of the slab sample. All measurements were carried out by rotating the angle θ from 0 ° to 360 ° under a specific H.

peaks of 275% and 732% at 2.7 and 3.2 T for 90 and 10 K, respectively. As for R_c, the maximal angle-dependent MR ratios of 90 and 10 K are 170% and 580% at $H = 2.7$ T and $H = 3.2$ T, respectively. At $H = 9$ T, the angle-dependent MR ratios monotonously decrease to ∼20% and ∼150% at 90 and 10 K. Further increasing H to 14 T, the oscillation of R disappears as shown in Fig. S9 [22]; thus the angle-dependent MR ratio becomes zero. Here it is noted that the maximal angle-dependent MR ratios in our samples are a few times larger than those in $La_{0.7}Ca_{0.3}MnO_3$ (80%) [11] and Sr_2IrO_4 (160%) [16], which is a very large value.

C. Origin of the large MR and angle-dependent MR

To gain a deeper understanding of the origin of large angle-dependent MR of $NaCrTe_2$, we calculated the electronic band structures and projected density of states (PDOS) of A-type AFM and both FM states by density functional theory with HSE06+U. Spin-orbit coupling is considered because of the heavy element Te. In Fig. 4(a), one can see that the band dispersion around E_F exhibits two-dimensional character with a flat band along H-K and large dispersive bands along K-Γ and M-Γ. An indirect band gap E_g, 0.39 eV, shows up between the Γ and M points, indicating that $NaCrTe_2$ is a semiconductor under the A-type AFM state. The metallic conductivity behavior shown in Fig. 2(a) may come from a little deficiency of Na. The electronic band structure and PDOS of Ising-like FM $NaCrTe_2$ are plotted in Fig. 4(b). Around E_F, the conduction bands along Γ-M and Γ-K are split wider, lowering the conduction band minimum (CBM) and slightly lifting the valence band maximum (VBM). Although the positions of CBM and VBM are unchanged, the E_g becomes narrower to be 0.11 eV. More interestingly, the valence band (VB) and conduction band (CB) are spin split because the VBM and CBM possess the same spin direction, respectively. It is insulating in a spin-down channel with spin-flip gaps $\Delta_1 = 0.4$ eV in VB and $\Delta_3 = 1.8$ eV in CB, and $\Delta_2 = E_g = 0.11$ eV in the spin-up channel. Thus the $NaCrTe_2$ changes into a FM half semiconductor under high H [27–29]. In Fig. S10 [22], we plotted the electronic band structure and PDOS of $NaCrTe_2$ under Ising-like FM and XY-like FM states using the PBE + U + SOC method. The band topology and DOS values near E_F are identical. Therefore, at $H > H_{sf2} > H_{sf1}$, the two FM states exhibit identical low-R states; see Fig. S9 [22]. The schematic changes of electronic band structure under H are shown in Figs. 4(c) and 4(d). Similar H-dependent conductivity is proposed in CrI_3, in which the change of spin alignment in turn alters the direct band gap (0.91 eV) into the indirect band gap (0.96 eV) and thus induces a large MR and angle-dependent MR ratio [30].

In addition, we observe two different transition trends from high-R to low-R states of $NaCrTe_2$ in Fig. 4(e). For $H \parallel c$, the high R value rapidly decreases to a low R value as H is close to H_{sf1}, while for $H \parallel ab$, the high-R state slowly approaches the low-R state as increasing H to H_{sf2}. Such kind of decrement leads to the difference in R exhibiting the maximal value at H_{sf1}, determining the largest magnitude of angle-dependent MR ratio. We calculated the MAE between two FM states,

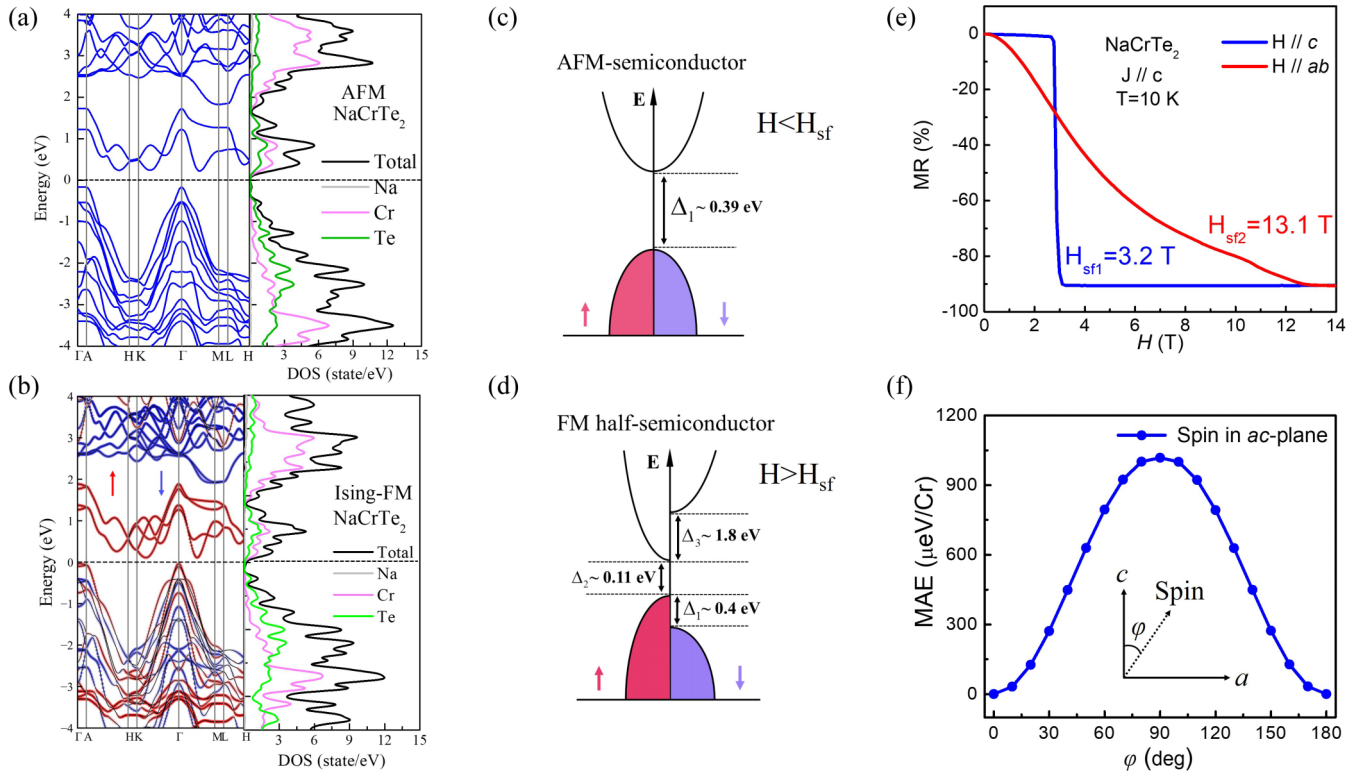

FIG. 4. Electronic structure and origin of giant angle-dependent MR. [(a),(b)] Band structure and PDOS of the A-type AFM and Ising-like FM $NaCrTe_2$ calculated by HSE06+U+SOC. [(c),(d)] Schematic electronic structure of A-type AFM semiconductor and FM half semiconductor under different H. (e) MR under $H \parallel c$ and $H \parallel ab$ at 10 K measured from 0 to 14 T. (f) MAE per Cr^{3+} of FM $NaCrTe_2$. In the inset, $\varphi = 0^\circ$ and 90 ° represent the Ising-like type and XY-like type FM configurations, respectively.

namely, rotating the spin direction rotates from the c axis ($\varphi = 0^\circ$, Ising-like type) to the a axis ($\varphi = 90^\circ$, XY-like type). In Fig. 4(f), it is found that the value of MAE $\xi_{\mathrm{MAE}} = E_{100} - E_{001}$ is 1017 μeV per Cr^{3+}, which theoretically explains the reason why flipping the the high-R state to the Ising-type low-R state is easier. It is noted that the MAE is considerably higher than those of known CrI_3 (650 μeV) [31,32], $Cr_2Ge_2Te_6$ (63 μeV) [33,34], and VI_3 (290 μeV) [35].

In a typical $La_{0.7}Ca_{0.3}MnO_3$ single crystal, there are no angle-dependent MR signals either in the pure AFM insulating phase or the H-induced FM metallic phase. The angle-dependent MR signal only emerges at the regime of MIT transition, and reaches a peak value at T close to T_{MIT}. It can be explained by the competing scenario between AFM insulator and FM metal, induced by Jahn-Teller distortion and double-exchange interaction, respectively [11]. However, the large angle-dependent MR ratio observed here is significantly different from other known CMR materials. In our work, the angle-dependent MR ratio shows a peak value at 10 K, far away from the T_N or T_c'. It recalls the angle-dependent MR effect in Sr_2IrO_4, where the largest ratio is found at the base temperature and around H_{sf}, where the spin-tuned conductivity drives the high-R state to the low-R state, leading to a negative MR and sizable angle-dependent MR ratio [14,15].

IV. CONCLUSION

Hence, the spin-flip-driven magnetotransports in $NaCrTe_2$ can be understood by the following two aspects. Firstly, the reduction of E_g from an AFM semiconductor to a FM half semiconductor is as large as 280 meV, which is a remarkably rare case. It reflects the strong coupling among spin, lattice, and conductivity in $NaCrTe_2$. This kind of change enhances the carrier concentration n and reduces R, which is the intrinsic origin of the large negative MR. Similarly, spin-flip transitions are observed in a layered A-type AFM CrSBr under H, and the strong coupling between spin and charge leads to negative MR signals of ~40% [36]. Secondly, the MAE between Ising-like-FM and XY-like-FM plays the most decisive role in producing angle-dependent MR signal because it directly determines the drop-off rate from the high-R state to the low-R state. Assuming that the MAE is very small, the decrement of R to either the Ising-like FM or XY-like FM low-R state would be nearly synchronous, and the angle-dependent MR ratio should be rather weak. Therefore, the reduced magnitude and the different descending in R conjointly determine the large angle-dependent MR effect. Our work deepens the understanding of origin for spin-related transport property in a layered antiferromagnet. More AFM-based materials exhibiting considerable magnetotransport effect are strongly expected.

ACKNOWLEDGMENTS

We thank Dr. Gang Xu and Dr. Zengwei Zhu for measuring the transport property at high magnetic field. This work was supported by the National Key Research and

Development Program of China (Grants No. 2017YFA0304700, No. 2016YFA0300600, No. 2018YFE0202601, and No. 2016YFA0300504), National Natural Science Foundation of China (Grants No. 51922105, No. 51772322, No. 11774423, and No. 11822412), Strategic Priority Research Program and Key Research Program of Frontier Sciences of the Chinese Academy of Sciences (Grant No. QYZDJ-SSW-SLH013), and Beijing Natural Science Foundation (Grant No. Z200005).

J.W. and J.D. contributed equally to this work.

[1] T. R. McGuige and R. I. Potter, IEEE Trans. Magn. **11**, 1018 (1975).
[2] T. Rijks, S. Lenczowski, R. Coehoorn, and W. de Jonge, Phys. Rev. B **56**, 362 (1997).
[3] F. Gorter, J. Potgiesser, and D. Tjaden, IEEE Trans. Magn. **10**, 899 (1974).
[4] M. M. Miller, G. A. Prinz, S. F. Cheng, and S. Bounnak, Appl. Phys. Lett. **81**, 2211 (2002).
[5] T. Jungwirth, X. Marti, P. Wadley, and J. Wunderlich, Nat. Nano. **11**, 231 (2016).
[6] V. Baltz, A. Manchon, M. Tsoi, T. Moriyama, T. Ono, and Y. Tserkovnyak, Rev. Mod. Phys. **90**, 015005 (2018).
[7] B. G. Park, J. Wunderlich, X. Martí, V. Holý, Y. Kurosaki, M. Yamada, H. Yamamoto, A. Nishide, J. Hayakawa, H. Takahashi, A. B. Shick, and T. Jungwirth, Nat. Mater. **10**, 347 (2011).
[8] X. Martí, B. G. Park, J. Wunderlich, H. Reichlová, Y. Kurosaki, M. Yamada, H. Yamamoto, A. Nishide, J. Hayakawa, H. Takahashi, and T. Jungwirth, Phys. Rev. Lett. **108**, 017201 (2012).
[9] D. Kriegner, K. Výborný, K. Olejník, H. Reichlová, V. Novák, X. Marti, J. Gazquez, V. Saidl, P. Němec, V. V. Volobuev, G. Springholz, V. Holý, and T. Jungwirth, Nat. Commun. **7**, 11623 (2016).
[10] Y. Ando, A. N. Lavrov, and S. Komiya, Phys. Rev. Lett. **90**, 247003 (2003).
[11] A. N. Lavrov, H. J. Kang, Y. Kurita, T. Suzuki, S. Komiya, J. W. Lynn, S. H. Lee, P. C. Dai, and Y. Ando, Phys. Rev. Lett. **92**, 227003 (2004).
[12] C. Wang, H. Seinige, G. Cao, J. S. Zhou, J. B. Goodenough, and M. Tsoi, Phys. Rev. X **4**, 041034 (2014).
[13] I. Fina, X. Marti, D. Yi, J. Liu, J. H. Chu, C. R. Serrao, S. Suresha, A. B. Shick, J. Železný, T. Jungwirth, J. Fontcuberta, and R. Ramesh, Nat. Commun. **5**, 4671 (2014).
[14] C. L. Lu, B. Gao, H. W. Wang, W. Wang, S. L. Yuan, S. Dong, and J. M. Liu, Adv. Funct. Mater. **28**, 1706589 (2018).
[15] N. Lee, E. J. Ko, H. Y. Choi, Y. J. Hong, M. Nauman, W. Kang, H. J. Choi, Y. J. Choi, and Y. J. Jo, Adv. Mater. **30**, 1805564 (2018).
[16] H. W. Wang, C. L. Lu, J. Chen, Y. Liu, S. L. Yuan, S. W. Cheong, S. Dong, and J. M. Liu, Nat. Commun. **10**, 2280 (2019).
[17] J. R. Carvajal, Phys. B (Amsterdam, Neth.) **192**, 55 (1993).
[18] G. Kresse and J. Furthmuler, Phys. Rev. B **54**, 11169 (1996).
[19] J. P. Perdew, K. Burke, and M. Ernzerhof, Phys. Rev. Lett. **77**, 3865 (1996).
[20] J. Heyd, G. E. Scuseria, and M. Ernzerhof, J. Chem. Phys. **118**, 8207 (2003).
[21] A. Togo and I. Tanaka, Scr. Mater. **108**, 1 (2015).
[22] See Supplemental Material at http://link.aps.org/supplemental/10.1103/PhysRevMaterials.5.L091401 for phonon spectra, energy of multiple magnetic structure, and magnetic and electrical transport measurement of single-crystal $NaCrTe_2$.
[23] S. Kobayashi, H. Ueda, C. Michioka, and K. Yoshimura, Inorg. Chem. **55**, 7407 (2016).
[24] Y. X. Peng, S. L. Ding, M. Cheng, Q. F. Hu, Y. J., F. G. Wang, M. Z. Xue, Z. Liu, Z. C. Lin, M. Avdeev, Y. L. Hou, W. Y. Yang, Y. Zheng, and J. B. Yang, Adv. Mater. **32**, 2001200 (2020).
[25] W. Bai, Z. Q. Hu, S. Wang, Y. Hua, Z. Sun, C. Xiao, and Y. Xie, Adv. Mater. **31**, 1900246 (2019).
[26] P. Wadley, V. Hills, M. R. Shahedkhah, K. W. Edmonds, R. P. Campion, V. Novák, B. Ouladdiaf, D. Khalyavin, S. Langridge, V. Saidl, P. Nemec, A. W. Rushforth, B. L. Gallagher, S. S. Dhesi, F. Maccherozzi, J. Železný, and T. Jungwirth, Nat. Commun. **4**, 2322 (2013).
[27] J. W. Yoo, C. Y. Chen, H. W. Jang, C. W. Bark, V. N. Prigodin, C. B. Eom, and A. J. Epstein, Nat. Mater. **9**, 638 (2010).
[28] V. N. Prigodin, N. P. Raju, K. I. Pokhodnya, J. S. Miller, and A. J. Epstein, Adv. Mater. **14**, 1230 (2002).
[29] N. S. Rogado, J. Li, A. W. Sleight, and M. A. Subramanian, Adv. Mater. **17**, 2225 (2005).
[30] P. H. Jiang, L. Li, Z. L. Liao, Y. X. Zhao, and Z. C. Zhong, Nano Lett. **18**, 3844 (2018).
[31] W. B. Zhang, Q. Qu, P. Zhu, and C. H. Lam, J. Mater. Chem. C **3**, 12457 (2015).
[32] J. L. Lado and J. F. Rossier, 2D Mater **4**, 035002 (2017).
[33] N. Z. Wang, H. B. Tang, M. Z. Shi, H. Zhang, W. Z. Zhuo, D. Y. Liu, F. B. Meng, L. K. Ma, J. J. Ying, L. J. Zou, Z. Sun, and X. H. Chen, J. Am. Chem. Soc. **141**, 17166 (2019).
[34] J. Y. You, Z. Zhang, X. J. Dong, B. Gu, and G. Su, Phys. Rev. Res. **2**, 013002 (2020).
[35] Y. P. Wang and M. Q. Long, Phys. Rev. B **101**, 024411 (2020).
[36] E. J. Telford, A. H. Dismukes, K. H. Lee, M. H. Cheng, A. Wieteska, A. K. Bartholomew, Y. S. Chen, X. D. Xu, A. N. Pasupathy, X. Y. Zhu, C. R. Dean, and X. Roy, Adv. Mater. **32**, 2003240 (2020).